

SCULPTING A PRE-PLANETARY NEBULA WITH A PRECESSING JET: IRAS 16342–3814

R. SAHAI,¹ D. LE MIGNANT,² C. SÁNCHEZ CONTRERAS,³ R. D. CAMPBELL,² AND F. H. CHAFFEE²

Received 2004 November 24; accepted 2005 February 11; published 2005 February 24

ABSTRACT

We have imaged the bipolar pre-planetary nebula IRAS 16342–3814 with the Keck adaptive optics (AO) system in four near-infrared bands in the 1.6–4.7 μm range. The lobes, which showed smoothly varying brightness distributions in previous optical images taken with the *Hubble Space Telescope*, have a limb-brightened appearance in the AO images, with a remarkable corkscrew structure inscribed on the lobe walls. A well-collimated, precessing jet with a diameter $\lesssim 100$ AU and a precession period $\lesssim 50$ yr, interacting with ambient circumstellar material, is most likely responsible for the corkscrew structure and the lobes, as indicated by a detailed comparison of our observations with published numerical simulations. The very red colors of the lobes in the near-infrared, coupled with their visibility at optical wavelengths, require that at least half, but not all, of the light of the central star be trapped by a compact circumstellar dust cloud heated to ~ 600 – 700 K and reradiated in the infrared. The lobes are thus illuminated both by the infrared light from this dust cloud as well as by the optical light from the central star.

Subject headings: circumstellar matter — ISM: jets and outflows — planetary nebulae: general — stars: AGB and post-AGB — stars: individual (IRAS 16342–3814) — stars: mass loss

1. INTRODUCTION

Collimated jets are one of the most intriguing, yet poorly understood phenomena in astrophysics. Jets have been found in a wide variety of object classes that include active galactic nuclei, young stellar objects, massive X-ray binaries (e.g., SS 433), black hole X-ray transients, symbiotic stars, supersoft X-ray sources, (possibly) recurrent novae, and, finally, planetary and preplanetary nebulae (PNs and PPNs, respectively). In the case of PNs and PPNs, wobbling collimated jets have been proposed as the universal mechanism that can shape the wide variety of bipolar and multipolar morphologies seen in these objects (Sahai & Trauger 1998, hereafter ST98; Sahai 2001).

The “water-fountain nebula,” IRAS 16342–3814 (hereafter IRAS 1634), belongs to a class of very young PPNs with high-velocity molecular outflows traced by radio H_2O and/or OH maser line emission (Likkell & Morris 1988). *Hubble Space Telescope* (*HST*) images of IRAS 1634 show a small bipolar nebula, with the lobes separated by a dark equatorial waist (Sahai et al. 1999a, hereafter S99). The image morphology was interpreted as bubble-like reflection nebulae illuminated by starlight escaping through polar holes in a dense, dusty waist obscuring the central star, with the bubbles created by a fast jetlike outflow plowing into the asymptotic giant branch (AGB) mass-loss envelope (S99). In this Letter, we report adaptive optics (AO) observations at near-infrared (near-IR) wavelengths that probe much deeper into the lobes and reveal a remarkable corkscrew-shaped structure apparently etched into the lobe walls. We interpret this “writing on the wall” as the signature of an underlying precessing jet, and we compare our results with predictions from numerical simulations of such jets.

2. OBSERVATIONS AND RESULTS

IRAS 1634 was imaged through the *H* (1.63 μm), *K_p* (2.12 μm), *L_p* (3.8 μm), and *M_s* (4.7 μm) filters on UT 2004 June 26 and 27 with the W. M. Keck II 10 m telescope using the near-infrared camera NIRC2 (K. Matthews et al. 2005, in preparation) with AO in its Natural Guide Star mode (Wizinowich et al. 2000). On each night, we observed IRAS 1634 1 hr around its transit (air mass ~ 1.9 – 2.0). The AO guide star, USN 0516-0460239, was located $10''.8$ west, $3''.5$ north from IRAS 1634. The AO system ran at its slowest speed (55 Hz) in a photon-starving regime (~ 50 counts per subaperture), delivering only a partial correction. On the best night (June 27), the seeing was $0''.45$ in the visible at an air mass of 2.0, as measured on the acquisition camera. The Strehl ratio (SR) was measured to be 0.22 in the AO guide star’s *K_p* images from June 27, giving a scaled SR of 0.40 (0.47) at the *L_p* (*M_s*) wavelength.

We present here the images and the photometry extracted from narrow field data ($9.94 \text{ mas pixel}^{-1}$, with a field of view of $10'' \times 10''$; see Fig. 1 and Table 1). The images in the different bands have been reduced in a standard way: sky-subtracted, flat-fielded, corrected for bad pixels, and shift-and-added in a final image for each observing setup. *L_p* and *M_s* images have been flux-calibrated using the photometric standard HD 161743 (Leggett et al. 2003) on UT June 26. *H* and *K_p* data have been flux-calibrated using NIRC2 photometric zero points.⁴

The *L_p* and *K_p* AO images are shown in Figure 1; the *M_s* image, with a significantly lower signal-to-noise ratio, and the *H*-band image, which looks very similar to the optical images, are not shown. All images reveal the same basic bipolar morphology for IRAS 1634 as seen in the optical *HST* images (S99); however, significant structure can be seen within the lobes in the *K_p* and *L_p* AO images. The *L_p* image shows this most clearly—in the E-lobe, bright emission knots E1, E2, E3, and E4 are seen straddling a bright corkscrew structure that extends from E1 to E4 (Fig. 2a). In the W-lobe, similar localized brightness features W1–W5 are seen; although a full corkscrew structure connecting these is not apparent, small extensions

¹ Jet Propulsion Laboratory, MS 183-900, California Institute of Technology, Pasadena, CA 91109; raghvendra.sahai@jpl.nasa.gov.

² W. M. Keck Observatory, 65-1120 Mamalahoa Highway, Kamuela, HI 96743.

³ California Institute of Technology, MS 105-24, Pasadena, CA 91125.

⁴ See <http://www2.keck.hawaii.edu/inst/nirc2>.

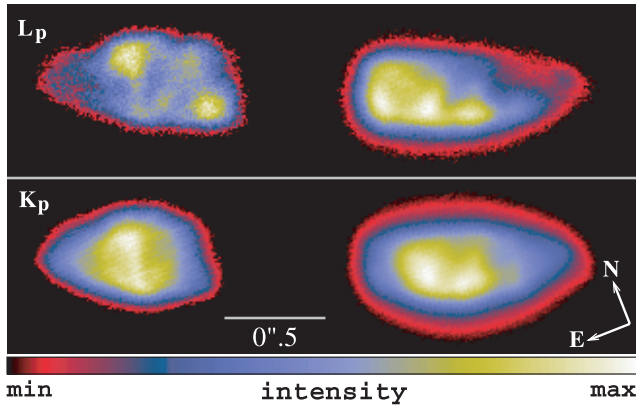


FIG. 1.—False-color AO images of IRAS 1634 in the L_p and K_p bands, shown with a linear stretch. The right half of the image, covering the west lobe (which is significantly brighter than the east lobe), has been scaled differently in order to show structures in both lobes clearly.

emanating from knots W2 and W3, as well as a low-contrast feature going from the top of W1 to the bottom of W2, indicate that parts of such a structure are most likely present. A three-color composite, made with the L_p and K_p AO images and the $0.8 \mu\text{m}$ *HST* image (from S99), is shown in Figure 2*b*. The *HST* image was registered relative to the AO images using nearby field stars. The thickness of the dark nebular waist between the lobes decreases with increasing wavelength. The lobes' position angle is clearly seen to rotate clockwise with increasing wavelength—this effect is most pronounced in going from the $0.8 \mu\text{m}$ image to the near-IR images.

The detailed shapes of the lobes do not have axial symmetry around a central axis; rather the curves defining the north (south) and south (north) boundaries of the E-lobe and W-lobe bear a point-symmetric relationship to each other. The change in the average position angle (P.A.) defining the lobes' long axis as a function of wavelength is another example of point symmetry. The overall lengths and widths of the two lobes are different, with the E-lobe being shorter and slightly wider.

3. THE BIPOLAR LOBES OF IRAS 1634

The limb-brightened structure of the lobes in the L_p image clearly shows that these are bubble-like structures with dense walls and tenuous interiors, as had been suggested by S99. Light from the central star is scattered into our line of sight by dust in the dense walls. The presence of bright regions E1–E4 and W1–W5 and the connecting corkscrew structure, most simply interpreted as regions of higher dust density producing enhanced scattered light emission, indicate that the walls are optically thin to scattering in the L_p wavelength band. Since some structure in the lobes can be seen in the K_p images also, but not in the H -band or shorter wavelength *HST* images (S99), it is likely that the transition from optical thickness to optical thinness occurs near $2 \mu\text{m}$. Since starlight reaching the walls penetrates roughly to an optical depth $\tau \sim 1$ before being scattered into our line of sight, and the optical depths are highest at $0.8 \mu\text{m}$, the lateral width of the lobes is smallest in the $0.8 \mu\text{m}$ image.

The observed change in the average P.A. with wavelength may be understood in terms of the lobe walls (1) being geometrically thicker and denser than average on the E-lobe's north side and the W-lobe's south side, and (2) having substantial optical depths at 0.8 and $2.1 \mu\text{m}$. This difference in structure

TABLE 1
AO OBSERVATIONS OF IRAS 1634

FILTER	λ_0 (μm)	FLUX (mJy)		FWHM (mas)	TIME (s)
		East	West		
H	1.63	24	59	45–60	10
K_p	2.12	35	86	47–55	120
L_p	3.78	104	234	82–85	210
M_s	4.67	165	245	96–100	280

will cause the lateral extent to be relatively more limited on the dense side at the shorter wavelengths, producing the observed differences in the lobes' average P.A.'s at different wavelengths.

The different lengths of the two lobes most likely result from the inclination of the dense dusty waist producing a larger obscuration of the E-lobe's inner parts (which is tilted away from us) than the W-lobe's inner parts. The difference in the widths of the E- and W-lobes is most likely related to intrinsic differences in the lateral sizes and structure of the cavities that define the lobes.

4. HOT DUST: THE CENTRAL ILLUMINATION SOURCE

We analyze the observed colors and intensities of the lobes at different wavelengths averaged over small patches (of size $0''.15$) located in the middle of the lobes (marked by crosses in Fig. 2), i.e., well removed from the lobe edges and the dense central waist, where the optical depths to scattered light are expected to be smallest. The colors result from a combination of reddening due to extinction, and blueing due to scattering, of light from the central illumination source. We have corrected our measured intensities for interstellar extinction using $A_V = 0.77$,

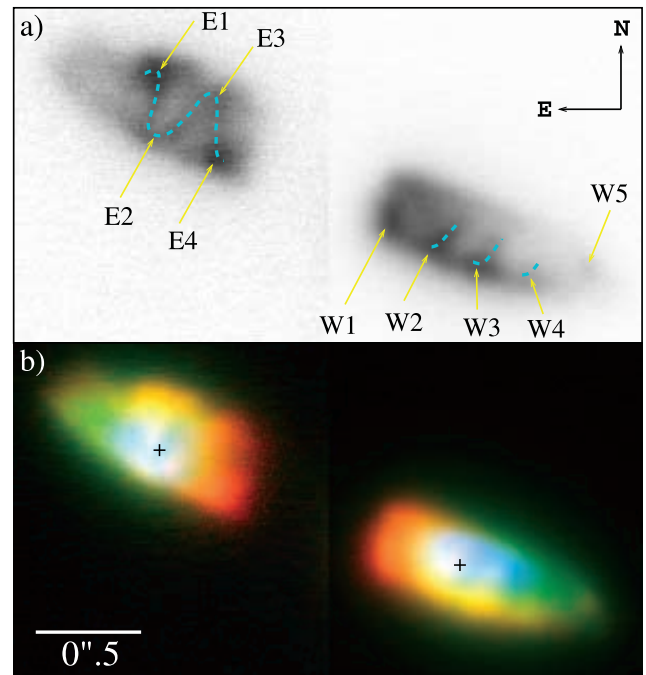


FIG. 2.—(a) L_p image of IRAS 1634, displayed on a linear stretch; dashed (cyan) curves delineate the corkscrew structure. (b) Color-composite image of IRAS 1634, made with the L_p (red), K_p (green), and $0.8 \mu\text{m}$ *HST* (blue) images, displayed on a linear stretch. Crosses mark the locations of regions used for analyzing the surface brightnesses in § 4. The right half of each image has been scaled differently from the left half, as in Fig. 1.

derived using the numerical algorithm provided by Hakkila et al. (1997), and a distance of 2 kpc (S99). In the W-lobe we find that the observed intensities for 2.1, 3.8, and 4.7 μm are 0.15, 0.5, and 0.73 Jy arcsec⁻², respectively, i.e., in the ratio 1 : 3.3 : 4.9, indicative of a very red source illuminating the lobes (the fainter E-lobe gives similar colors).

We now show that the central source responsible for most of the scattered light in the near-IR is most likely hot dust, as has been inferred for the bipolar PPN, OH 231.8+4.2 (e.g., Kastner & Weintraub 1995). We do not think that line emission has a significant contribution to the emission seen in the near-IR or optical filters—García-Hernández et al. (2002) report that optical and near-IR spectroscopy shows no line emission (e.g., in the 2.12 μm H₂, H α , Br γ , and Br α lines). We have modeled the K_p , L_p , and M_s surface brightnesses (allowing $\pm 30\%$ errors), varying the illuminating blackbody's luminosity, L_d , and temperature, T_d , using equation (1) [with $y = 1$ and τ_{los} replaced by the more general form $1 - \exp(-\tau_{\text{los}})$] and equation (2) from Sahai et al. (1999b). We find that a fit can be obtained only with $L_d \geq 6000(D/2 \text{ kpc})^2 L_\odot$ and $T_d \sim 600\text{--}700$ K, using extrapolated dust opacities at the L_p and M_s wavelengths derived from power-law fits to the dust opacities at the H and K bands ($\tau_e \propto \lambda^{-2}$ and $\tau_s \propto \lambda^{-3.7}$) from Whitney (1995; model 1). With a less steep extinction power law $\tau_e \propto \lambda^{-1.5}$ (but the same albedos as in model 1), we can fit the IRAS 1634 data with $L_d \geq 3000(D/2 \text{ kpc})^2 L_\odot$ and $T_d \sim 700$ K (model 2). The scattering optical depths depend on L_d —e.g., for $L_d = 6100\text{--}3100 L_\odot$, $\tau_{\text{los}} = 1.6\text{--}0.76$, $0.24\text{--}0.11$, and $0.22\text{--}0.11$, at 2.1, 3.8, and 4.7 μm , respectively. Since the total estimated luminosity of IRAS 1634 is $L_* \sim 6000(D/2 \text{ kpc})^2$, and since the observed surface brightnesses in the *HST* images at 0.55 and 0.81 μm require a central optical light source of at least $\sim 650 L_\odot$, model 2 is more plausible than model 1; i.e., the power law characterizing the 2–5 μm extinction is shallower than λ^{-2} . Based on model 2, we conclude that at least half, but not all, of the central star's light is absorbed by a compact circumstellar dust cloud. The lobes are thus illuminated partially by near-IR light from the dust cloud heated to $T_d \sim 600\text{--}700$ K and partially by optical light from the central star.

An upper limit to the characteristic radius of the central dust cloud source can be estimated as $r_d = (L_* T_*^p / 16\pi\sigma)^{1/2} T_d^{-(2+p/2)}$ (Herman et al. 1986), giving $r_d \sim 40\text{--}110$ AU for $L_* = 6000 L_\odot$, $T_* = 2500\text{--}10,000$ K, $T_d = 650$ K, and the dust power-law absorptivity index $p = 1.5$ (σ is the Stefan-Boltzmann constant). A lower limit, $r_d \geq 30(6000 L_\odot / L_d)^{1/2}$ AU, comes from assuming that the 650 K dust cloud reradiates all of the absorbed luminosity (L_d) like a blackbody. This hot dust cloud most likely heats the dust in the dense equatorial torus and spherical AGB mass-loss envelope to temperatures of ≤ 100 K, producing the far-IR emission seen by the *Infrared Space Observatory* and the *Infrared Astronomical Satellite* (IRAS; Dijkstra et al. 2003; S99).

5. IRAS 1634 AND THE FORMATION OF ASPHERICAL PLANETARY NEBULAE

In S99, we concluded that IRAS 1634 shows strong evidence of ST98's hypothesis that fast collimated outflows with changing directionality are the primary agent for setting the stage in the formation and shaping of PNs, rather than a preexisting equatorial density enhancement in the AGB circumstellar envelope (CSE), as assumed in the once popular generalized interacting winds model (Balick 1987; Balick & Frank 2002). This evidence was the presence of (1) a collimated high-velocity wind, shaping

(2) a point-symmetric imprint (i.e., the bipolar nebula) in a surrounding dense AGB CSE. In ST98's model, the large dense equatorial torus in IRAS 1634 and other bipolar PPNs is not responsible for collimating the fast jetlike outflows but may play a limited hydrodynamical role in defining the lobe geometry at low latitudes.

The corkscrew structure seen in the lobes of IRAS 1634 now strongly suggests that the collimated high-velocity wind is a precessing jet. We do not see the jet beam directly but via its interaction with the ambient circumstellar medium that produces a compressed structure of enhanced density in the shape of a corkscrew. A similar example of a corkscrew structure has recently been found in SS 433 (Margon 1984; Blundell & Bowler 2004), which has long been known to harbor a bipolar, relativistic precessing jet. A precessing jet has been inferred in another water-fountain PPN, W43A, from fitting the distribution of high-speed H₂O maser emission knots in this object (Imai et al. 2002), and in the symbiotic star CH Cyg, on the basis of its radio nebula's changing P.A. (Crocker et al. 2002).

Although very little work has been done on numerical simulations of precessing jets interacting with circumstellar envelopes, Cliffe et al. (1995, hereafter CFLJ95) modeled an episodic, precessing jet interacting with a uniform density interstellar medium. Their simulation produced bright S-shaped features on the surface of a bubble-shaped polar lobe: the latter resulted from the bow shocks of the individual jet segments merging into a single “global” shock structure that enveloped the entire complex of segments. Although radiative cooling is not included (but is likely to be important in IRAS 1634 where the lack of shocked gas emission [see § 4] implies strong cooling), the influence of radiative losses is not expected to alter the general morphology (CFLJ95). Thus, both the corkscrew structure and the lobes were produced by the precessing jet. Alternatively, the lobes may be preexisting structures with the jet inscribing a corkscrew signature on their walls (as, e.g., has been proposed for the PN, M2-9, by Doyle et al. 2000). But this is a more complex scenario, as it requires a preceding collimated fast-wind episode that creates the lobes, and hydrodynamical simulations of such a model are needed to quantitatively test its viability. Our inferences below regarding jet properties do not depend on the adopted model.

The continuous appearance of the observed corkscrew structure in IRAS 1634 indicates that its jet has operated quasi-continuously, at least for an interval of about 1.5 precessional periods represented by the corkscrew's extent from E1 to E4. The jet precession period, τ_p , can be estimated from the time interval, t_{exp} , required by the jet-compressed material to traverse the distance (l_p) between successive locations in the corkscrew pattern separated by one precessional period, e.g., E1 and E3, E2 and E4 in the E-lobe and W1 and W2, W2 and W3 in the W-lobe. The average value of l_p in the E-lobe (W-lobe) is 0'33 (0'23). Making the reasonable assumption that the intrinsic outflow speed of the compressed material in the corkscrew pattern is comparable to that measured for the OH masers derived by S99, $67 \text{ km s}^{-1} / \cos i \sim 90 \text{ km s}^{-1}$, where $i \sim 40^\circ$ is the inclination of the symmetry axis to the line of sight, $t_{\text{exp}} = (l_p D / \sin i) / 90 \text{ km s}^{-1}$, where D is the distance to the nebula. Taking $D = 2 \text{ kpc}$ (S99) and $l_p = 0'28$, we find $\tau_p \lesssim 50 \text{ yr}$ —the upper limit results from the likely possibility that the material in the corkscrew has been decelerated by the surrounding ambient medium. The value of τ_p is (1) consistent with the dynamical timescale of the H₂O masers in IRAS 1634 (150 yr), which are located just beyond the lobe tips, with a separation of 2'97 along P.A. = 66° (Claussen et al. 2004),

and (2) not very different from that of W43A (55 yr; Imai et al. 2002). The main difference between the CFLJ95 model and IRAS 1634 is due to the much longer precession period of the model jet (3.6×10^4 yr) but comparable jet velocity—the model lobe’s linear extent (4.5 pc) is much larger, and the model corkscrew pattern is less tightly wound. Since the CFLJ95 model lobes appear to be significantly less collimated than those in IRAS 1634, the jet precession cone half-angle jet in the latter must be significantly smaller than the model value (26°), plausibly as small as in W43A (5° ; Imai et al. 2002).

Even though the jet beam is not directly observed, we can infer an upper limit on the jet beam’s diameter from the corkscrew pattern’s thickness (since the compressed material resulting from the action of the jet on the ambient medium will, in general, expand and spread). The thickness, measured from a radial intensity cut along the lobes, is $\leq 0''.09$ (180 AU at 2 kpc). Using CFLJ95’s model, in which the jet diameter is about half the corkscrew pattern’s width, it is plausible that the jet beam in IRAS 1634 has an intrinsic diameter of ≤ 100 AU. Free thermal expansion of the jet from its launch point to where it first interacts with ambient gas can be ignored because the jet speed is likely to be quite fast (approximately a few times 100 km s^{-1}) compared to the sound speed of the jet gas ($\leq 10 \text{ km s}^{-1}$) for $T \leq 10^4 \text{ K}$.

The specific differences between the lobes (e.g., in the lobe widths, the appearance of the corkscrew structures) must be related to differences in the properties of (1) the jet outflows on the different sides of the nebula (e.g., in speed, opening angle, mass flux) and/or (2) the ambient circumstellar material (e.g., density).

The formation of jets in dying stars in general, and in IRAS 1634 in particular, is likely to involve the presence of an accretion disk. A favored model for producing such disks relies on the gravitational interaction of the mass-losing evolved star with a compact companion (Soker & Livio 1994). In this model, the precession of the jet is most likely driven by disk precession. Using the relationship between disk precession and binary rotation period given by CFLJ95, $\tau_b/\tau_p = \frac{3}{4}[q/(1+q)^{0.5}] \times$

$(R_{\text{disk}}/a)^{1.5}$ (where q is the mass ratio, taken to be ~ 1), and assuming that the disk radius, R_{disk} , and the binary separation, a , are comparable, τ_b is comparable to τ_p , i.e., ≤ 50 yr. Assuming a combined mass of $1 M_\odot$ for the binary, the above τ_p implies a separation $a \leq 10 \text{ AU}$.

We think it is unlikely that the proposed accretion disk around the companion is the location of the hot dust cloud inferred in § 4, first because of the discrepancy in their estimated sizes and second because the dust cloud must cover a substantial fraction of the solid angle around the central star since it absorbs a very large fraction of the stellar luminosity. The dust cloud is likely to be a cocoon that surrounds the star, with polar holes that may have been created by the precessing jet, similar to that inferred for another PPN, CRL 2688 (Sahai et al. 1998).

Our discovery of the corkscrew pattern resulting from a precessing jet in IRAS 1634 is an exciting addition to our knowledge of jets in dying stars as well as astrophysical jets in general. New AO imaging at a later epoch a few years from now should enable us to measure proper motions in the corkscrew pattern and should provide strong constraints on detailed numerical models of the nebular-shaping process. Deep optical spectroscopy of the lobes is critically needed to study the spectrum of the central star (reflected from the lobe walls), possibly leading to a spectroscopic detection of its inferred companion (as, e.g., in OH 231.8+4.2; Sánchez Contreras et al. 2004).

We thank Noam Soker, Adam Frank, and Joel Kastner for reading and commenting on early versions of this Letter. The data presented herein were obtained at the W. M. Keck Observatory, which is operated as a scientific partnership among the California Institute of Technology, the University of California, and NASA. The Observatory was made possible by the generous financial support of the W. M. Keck Foundation. R. S. is thankful for partial financial support for this work from a NASA/ADP grant (RTOP 399-20-00-08). C. S. C. is supported by the National Science Foundation through grant 9981546 to the Owens Valley Radio Observatory.

REFERENCES

- Balick, B. 1987, *AJ*, 94, 671
 Balick, B., & Frank, A. 2002, *ARA&A*, 40, 439
 Blundell, K. M., & Bowler, M. G. 2004, *ApJ*, 616, L159
 Claussen, M., Sahai, R., & Morris, M. 2004, *ASP Conf. Ser.* 313: *Asymmetrical Planetary Nebulae III: Winds, Structure and the Thunderbird*, ed. M Meixner, J. H. Kastner, B. Balick, & N. Soker (San Francisco: ASP), 331
 Cliffe, J. A., Frank, A., Livio, M., & Jones, T. W. 1995, *ApJ*, 447, L49 (CFLJ95)
 Crocker, M. M., Davis, R. J., Spencer, R. E., Eyres, S. P. S., Bode, M. F., & Skopal, A. 2002, *MNRAS*, 335, 1100
 Dijkstra, C., Waters, L. B. F. M., Kemper, F., Min, M., Matsuura, M., Zijlstra, A., de Koter, A., & Dominik, C. 2003, *A&A*, 399, 1037
 Doyle, S., Balick, B., Corradi, R. L. M., & Schwarz, H. E. 2000, *AJ*, 119, 1339
 García-Hernández, D. A., Manchado, A., García-Lario, P., Domínguez-Tagle, C., Conway, G. M., & Prada, F. 2002, *A&A*, 387, 955
 Hakkila, J., Myers, J. M., Stidham, B. J., & Hartmann, D. H. 1997, *AJ*, 114, 2043
 Herman, J., Burger, J. H., & Penninx, W. H. 1986, *A&A*, 167, 247
 Imai, H., Obara, K., Diamond, P. J., Omodaka, T., & Sasao, T. 2002, *Nature*, 417, 829
 Kastner, J., & Weintraub, D. A. 1995, *AJ*, 109, 1211
 Leggett, S. K., et al. 2003, *MNRAS*, 345, 144
 Likkell, L., & Morris, M. 1988, *ApJ*, 329, 914
 Margon, B. 1984, *ARA&A*, 22, 507
 Sahai, R. 2001, in *Post-AGB Objects as a Phase of Stellar Evolution*, ed. R. Szczerba & S. K. Górný (Ap&SS Libr. Vol. 265; Dordrecht: Kluwer), 53
 Sahai, R., te Lintel Hekkert, P., Morris, M., Zijlstra, A., & Likkell, L. 1999a, *ApJ*, 514, L115 (S99)
 Sahai, R., & Trauger, J. T. 1998, *AJ*, 116, 1357 (ST98)
 Sahai, R., et al. 1998, *ApJ*, 493, 301
 Sahai, R., Zijlstra, A., Bujarrabal, V., & te Lintel Hekkert, P. 1999b, *AJ*, 117, 1408
 Soker, N., & Livio, M. 1994, *ApJ*, 421, 219
 Sánchez Contreras, C., Gil de Paz, A., & Sahai, R. 2004, *ApJ*, 616, 519
 Whitney, B. 1995, *Rev. Mex. AA Conf. Ser.*, 1, 201
 Wizinowich, P., et al. 2000, *PASP*, 112, 315